Dynamic visualization of RANKL and Th17-mediated osteoclast function

Junichi Kikuta,[1,2] Yoh Wada,[3] Toshiyuki Kowada,[4] Ze Wang,[5] Ge-Hong Sun-Wada,[3] Issei Nishiyama,[1,2] Shin Mizukami,[4,6] Nobuhiko Maiya,[7] Hisataka Yasuda,[8] Atsushi Kumanogoh,[9] Kazuya Kikuchi,[4,6] Ronald N. Germain,[5] and Masaru Ishii[1,2]

[1]Laboratory of Cellular Dynamics, WPI–Immunology Frontier Research Center, Osaka University, Osaka, Japan. [2]Japan Science and Technology, CREST, Tokyo, Japan. [3]Division of Biological Sciences, Institute of Scientific and Industrial Research, and [4]Laboratory of Chemical Imaging Techniques, WPI–Immunology Frontier Research Center, Osaka University, Osaka, Japan. [5]Lymphocyte Biology Section, Laboratory of Systems Biology, National Institute of Allergy and Infectious Diseases, NIH, Bethesda, Maryland, USA. [6]Department of Material and Life Sciences, Graduate School of Engineering, Osaka University, Osaka, Japan. [7]Instruments Co., Nikon Corp., Kanagawa, Japan. [8]Planning and Development Group, Bioindustry Division, Oriental Yeast Co., Tokyo, Japan. [9]Department of Respiratory Medicine, Allergy and Rheumatic Disease, Graduate School of Medicine, Osaka University, Osaka, Japan.

Osteoclasts are bone resorbing, multinucleate cells that differentiate from mononuclear macrophage/monocyte-lineage hematopoietic precursor cells. Although previous studies have revealed important molecular signals, how the bone resorptive functions of such cells are controlled in vivo remains less well characterized. Here, we visualized fluorescently labeled mature osteoclasts in intact mouse bone tissues using intravital multiphoton microscopy. Within this mature population, we observed cells with distinct motility behaviors and function, with the relative proportion of static – bone resorptive (R) to moving – nonresorptive (N) varying in accordance with the pathophysiological conditions of the bone. We also found that rapid application of the osteoclast-activation factor RANKL converted many N osteoclasts to R, suggesting a novel point of action in RANKL-mediated control of mature osteoclast function. Furthermore, we showed that Th17 cells, a subset of RANKL-expressing CD4$^+$ T cells, could induce rapid N-to-R conversion of mature osteoclasts via cell-cell contact. These findings provide new insights into the activities of mature osteoclasts in situ and identify actions of RANKL-expressing Th17 cells in inflammatory bone destruction.

Introduction

Bone is a highly dynamic organ that is continuously being remodeled by the cooperative action of osteoclasts that resorb old bone and osteoblasts that create new bone. Osteoclasts are giant polykaryons differentiated from monocyte/macrophage-lineage hematopoietic precursor cells termed *osteoclast precursors*. Previous studies have revealed key molecular signals, such as those mediated by M-CSF and RANKL, which regulate the differentiation of these cells (1, 2). When cultured in the presence of M-CSF and RANKL, monocytoid cells isolated from bone marrow can successfully be differentiated into multinucleated giant cells in vitro, called *osteoclast-like cells*. However, the osteoclast-like cells generated in vitro often contain more than 100 nuclei (3), and it remains unclear whether such extraordinarily large polykaryons are formed in vivo, except in some pathological conditions such as Paget disease and giant cell tumors (4, 5). Furthermore, how the activity of multinucleate osteoclasts is controlled in vivo once they form remains largely unexplored. To address these issues and advance our understanding of this critical cell population with respect to bone homeostasis and osteopathology, we utilized intravital multiphoton microscopy (6–8).

Fully differentiated osteoclasts can adhere to bone surfaces and tightly seal the attachment areas with a characteristic membrane structure referred to as the "ruffled border" (Supplemental Figure 1A; supplemental material available online with this article; doi:10.1172/JCI65054DS1). A large number of vacuolar H$^+$–ATPases (V-type H$^+$-ATPases) are expressed along the ruffled border membrane in mature osteoclasts; these enzymes are responsible for secreting extraordinarily high numbers of protons, leading to acid resorption of the hard bone minerals (9, 10). V-type H$^+$-ATPase consists of multiple subunits, and each subunit has several isoforms; among them the a3 isoform of the *a* subunit is abundantly expressed in osteoclasts and is thus suitable as a marker for identifying mature osteoclasts (Supplemental Figure 1B and refs. 11, 12). In this study, by exploiting fluorescent reporter mice where GFP is expressed under the promoter of V-type H$^+$-ATPase a3 subunit (a3-GFP mice), we have succeeded in visualizing fluorescently labeled mature osteoclasts in live bones using intravital multiphoton microscopy. Based on such imaging, we have identified 2 different populations of mature osteoclasts in situ, corresponding with the static – bone resorptive (R) and moving – nonresorptive (N) fractions, with the transition between these states critically controlled by RANKL and showing a strong correlation to the state of cell motility. Our findings also revealed that RANKL-expressing Th17 regulates the status of mature osteoclasts by direct cell-cell contact, identifying what we believe is a novel mechanism of Th17-mediated inflammatory bone destruction.

Results

To label mature osteoclasts fluorescently, we modified the mouse *Tcirg1* locus, encoding the V-type H$^+$-ATPase a3 subunit, to produce a GFP fusion protein. Embryonic stem cell–mediated gene targeting was used to generate mice in which an a3 subunit-GFP fusion protein is expressed under the original promoter of the a3 subunit (a3-GFP mice) (13). Using bone tissue sections from these mice, we confirmed that tartrate-resistant acid phosphatase–positive (TRAP-positive) mature osteoclasts express GFP (Supplemental Figure 1C).

Conflict of interest: The authors have declared that no conflict of interest exists.

Citation for this article: *J Clin Invest.* doi:10.1172/JCI65054.

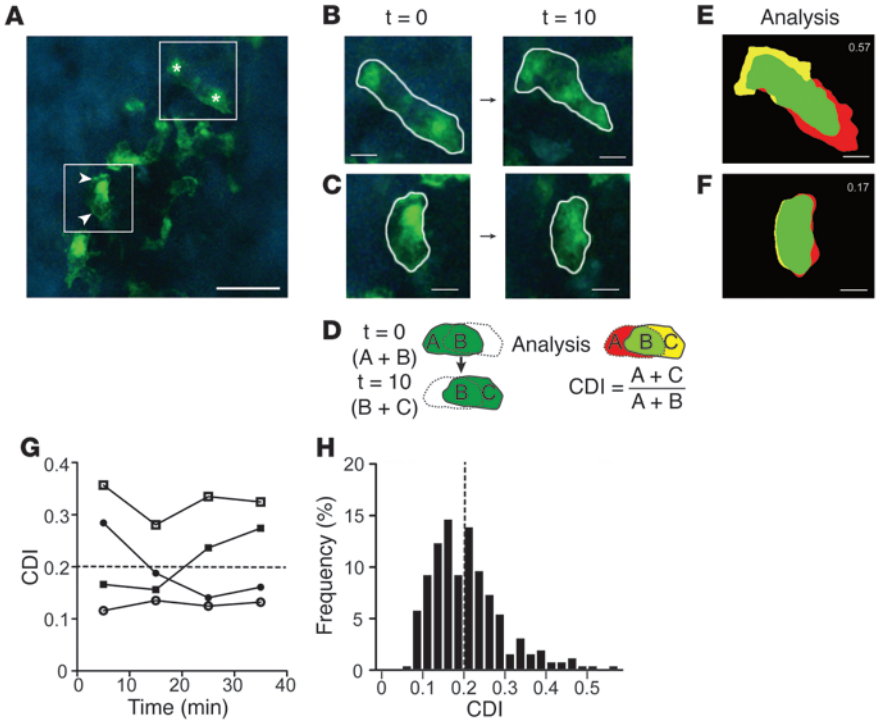

Figure 1
Visualization of living mature osteoclasts on the endosteum by using intravital multiphoton microscopy. (**A**) A representative image of live bone imaging of a3-GFP mice in control conditions. Green, mature osteoclasts expressing GFP-fused V-type H^+-ATPase a3 subunit; blue, bone surface. Scale bar: 40 μm. Arrowheads and asterisks represent surface and cytoplasmic distribution of V^-type H^+-ATPase a3 subunit, respectively. (**B** and **C**) Magnified images of 2 types of representative mature osteoclasts. White lines, cell borders. Scale bars: 10 μm. (**D**) Cell shapes were automatically recognized by the image analysis software, and 3 distinct areas were defined: occupied in the initial time frame (t = 0) (**A**, red), occupied in the final time frame (t = 10) (**C**, yellow), and overlapping between the 2 time frames (**B**, green). CDI was calculated as (A+C)/(A+B), representing the ratio of areas changed during 10 minutes divided by total cell area at t = 0 (see details in Supplemental Figure 2). (**E** and **F**) Processed images for CDI calculation (**E** for **B**, and **F** for **C**, respectively). Actual values of CDI were shown in upper right corners in **E** and **F**. Scale bars: 10 μm. (**G**) Examples of time-dependent transitions of CDIs. Each symbol represents a different cell tracked over a period of 40 minutes. Some cells changed their CDIs from lower to higher or vice versa (black symbols), whereas others remained in the similar CDI (white symbols). (**H**) Histogram of CDIs of mature osteoclasts under control conditions (n = 259, collected from 5 independent experiments).

By performing intravital multiphoton microscopy of calvaria in a3-GFP knockin mice, we could visualize live mature osteoclasts on the endosteum (Figure 1A and Supplemental Video 1). This live imaging identified a population of large multinuclear GFP^+ osteoclasts on the bone surface that showed substantial heterogeneity in terms of their amoeboid movements, including populations at the ends of a distribution of motilities that we could label as "moving" (Figure 1B) and "relatively static" (Figure 1C). These designations were derived from a quantitative analysis of osteoclast movement on the bone surface based on new image analysis software we developed for tracking the time-dependent morphological changes of these cells (Figure 1, D–F, Supplemental Figure 2, and Supplemental Video 2). Cell shapes were automatically recognized by the image analysis software before and after a certain period of time (10 minutes) (Supplemental Figure 2 and Supplemental Video 2), and 3 distinct areas were defined: occupied only in the initial time frame (t = 0) (A), occupied only in the final time frame (t = 10) (C), and overlapping at the initial and final points (B) (Figure 1D and Supplemental Figure 2). A cell deformation index (CDI) was calculated as the ratio (A + C)/(A + B). If the cells were moving vigorously, the area of overlap at the 2 time points (B area) would be small, leading to a higher CDI (Figure 1E), whereas in osteoclasts showing less movement, almost all the area would overlap at the 2 time points, area B would be larger, and the CDI would be lower (Figure 1F).

Because GFP is expressed as a fusion protein with the a3 subunit, GFP fluorescence not only serves as a marker for mature osteoclasts, but it may also provide information on the subcellular distribution of V-type H^+-ATPase in mature osteoclasts if sufficient spatial resolution could be achieved. Because the a3 subunit is an indispensable constituent of the V-type H^+-ATPase pump, connecting transmembrane (V0) and intracellular (V1) portions (14), and is well documented as being involved in H^+ secretion in osteoclasts as well as in other macrophage-lineage cell types (11, 12, 15), it is reasonable to assume that the subcellular distribution of this molecule reflects the functional state of this H^+ pump.

In the 2 polar examples shown in Figure 1, B and C, the different distributions of GFP–V^-type H^+-ATPase are obvious. Static osteoclasts had the ATPase distributed along the sealing zone membranes (Figure 1A), suggesting that they were actively engaged in bone resorption. On the other hand, in osteoclasts undergoing amoeboid movement, the V^-type H^+-ATPases seemed to be distributed diffusely in the cytoplasm (Figure 1A), suggesting these cells would be ineffective at resorption at this moment. Although the distributional changes of GFP–V^-type H^+-ATPases were not necessarily obvious in all osteoclasts imaged due to the limited spatiotemporal resolution of intravital multiphoton bone imaging, it is reasonable from these considerations to consider mobility to be associated with function, i.e., static and moving osteoclasts were resorptive and nonresorptive, respectively. During extended imaging (~40 minutes), some cells changed their CDIs from lower to higher or vice versa (Figure 1G), whereas others remained in a similar CDI state (Figure 1G). These data imply that osteoclasts change their functional activity over time in concert with changes in their motility.

A histogram of CDIs calculated from imaging more than 250 different mature osteoclasts revealed a broad distribution with a wide peak from 0.16 to 0.24 CDI (Figure 1H). Previous reports implied the existence of distinct subsets of mature osteoclasts in terms of their resorptive activity (16). Our imaging data based on tracking a functional reporter (V-type H^+-ATPase) agree with this previous report and characterize these different populations of

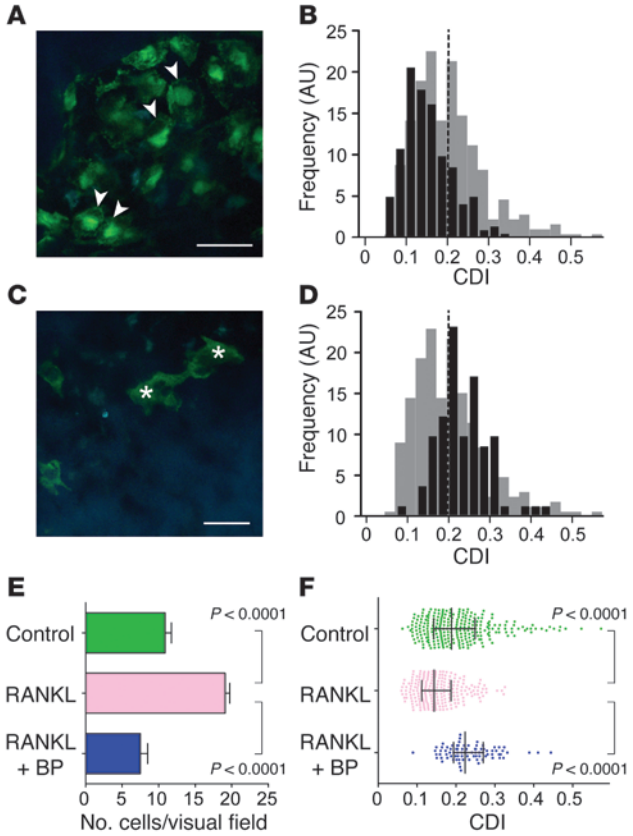

Figure 2
Visualization of mature osteoclasts under pathophysiological conditions. (**A** and **B**) A representative image of live bone imaging of a3-GFP mice after RANKL application (**A**, Supplemental Video 3). Arrowheads indicate a3-GFP at peripheral cell membrane. Scale bar: 40 μm. Histogram of CDIs for osteoclasts imaged under RANKL treatment conditions (black) and control conditions (gray, same as in Figure 1H) (**B**) (n = 224, collected from 5 independent experiments). (**C** and **D**) Representative depiction of live bone imaging of a3-GFP mice after application of RANKL and risedronate (**C**, Supplemental Video 4). Asterisks indicate a3-GFP in cytoplasm. Scale bar: 40 μm. Histogram of the CDIs for osteoclasts imaged under RANKL plus risedronate-treatment conditions (black) and under control conditions (gray, same as in Figure 1H) (**D**) (n = 82, from 5 independent experiments). (**E**) Total number of mature osteoclasts. from 5 independent experiments. (**F**) Distribution of CDI. Data points (n = 259 for control, n = 224 for RANKL, and n = 82 for RANKL plus risedronate) represent individual cells compiled from 5 independent experiments. Error bars represent medians ± interquartile range.

mature osteoclasts as (a) R, (b) N, and (c) intermediate, presumably corresponding to cells actively undergoing a change in state on the bone surface in vivo.

Pretreatment of mice with recombinant RANKL stimulates osteoclastogenesis and reduces bone tissue density (17, 18). In animals treated with this cytokine for 2 days, the total number of mature osteoclasts was increased (Figure 2A and Supplemental Video 3). The CDI histogram showed a left-shifted distribution generally corresponding to the lower end of the motility distribution for cells analyzed under control conditions (Figure 2B), representing an increase in the R population. This interpretation was further supported by the observation that almost all the static osteoclasts showed cell surface expression of GFP–H^+ -ATPases in that condition (Figure 2A). On the other hand, application of risedronate, a bisphosphonate (19, 20) used therapeutically to block bone resorption, reduced the total number of mature osteoclasts tightly attached to the bone surface, with many of the remaining cells showing cytoplasmic GFP expression (Figure 2C, and Supplemental Video 4) and with a CDI distribution skewed to the right (Figure 2D), representing an increase in the N population. Statistical analyses demonstrated that treatment with RANKL or RANKL plus bisphosphonate each changed both the total number (Figure 2E) and also significantly altered the CDI distribution (Figure 2F) of mature osteoclasts in vivo. In summary, intravital imaging of mature osteoclasts accompanied with quantitative analyses with CDI enabled us to visualize the functional states as well as the number of mature bone-resorbing osteoclasts in vivo.

To further analyze the different populations of mature osteoclasts, we also generated a chemical fluorescent probe detecting bone resorption at local sites on the bone surface (Supplemental Figure 3A). BAp-E, a boron-dipyrromethene–based (BODIPY-based) H^+-sensing fluorescent probe (pKa ~ 6.2) was conjugated with alendronate, a bisphosphonate, to promote adherence to bone surfaces. The probe coats the bone surface once administered, and green fluorescent signals are detected along the bone surface when mature osteoclasts secrete H^+ for bone resorption and the local pH is decreased. The fluorescence quantum yield (Φ) at pH 7.5 was 0.039, and the Φ at pH 6.0 was 0.29 (the pKa of the fluorescence of the probe was 6.2). Thus, an approximately 7.4-fold increase in fluorescence can be observed for pH changes of this extent (21). We administered this probe to mice in which tdTomato, a red fluorescent protein, is expressed under the promoter of TRAP, a well-known marker for mature osteoclasts (Supplemental Figure 3B). We observed large TRAP-positive (tdTomato) cells on the bone surface, representing mature osteoclasts (Figure 3, A and C, and Supplemental Video 5). Again, we detected 2 different types of labeled osteoclasts in terms of motility, moving (Figure 3A), and static (Figure 3A). Consistent with the data presented above using the GFP–V-type H^+-ATPase–marked cells, green fluorescent signals from the H^+ probes (Figure 3B) overlapped with static but not moving osteoclasts (Figure 3, C and D), supporting the idea that former cells are secreting protons actively and resorbing bone tissues when observed in vivo. We also noticed that there were green dots representing low pH that did not overlap with red osteoclasts (Figure 3C). We think these signals may represent areas previously undergoing active resorption by mature osteoclasts but not covered by osteoclasts at the time of imaging. This interpretation is consistent with in vitro data showing that pitted areas on the bone surface are not always colocalized with osteoclasts (22).

Using these new imaging tools, we next examined the short-term effect of RANKL on the function of mature osteoclasts (Figure 4). Interestingly, less than 10 minutes after i.v. injection of recombinant GST-RANKL, we found that many moving osteoclasts became static cells, suggesting an N-to-R transition without any change in the total number of mature osteoclasts (Figure 4, B and C, and Supplemental Video 6). Because this time course was much faster than that believed required for differentiation or maturation of new osteoclasts in the presence of RANKL, these data indicate that RANKL may have the unexpected property of converting existing mature N into mature R osteoclasts. This concept is compatible with previous literature describing a prompt increase (within 1 hour) in the level of ionized calcium in blood in RANKL-treated mice (23). A lower dose of RANKL

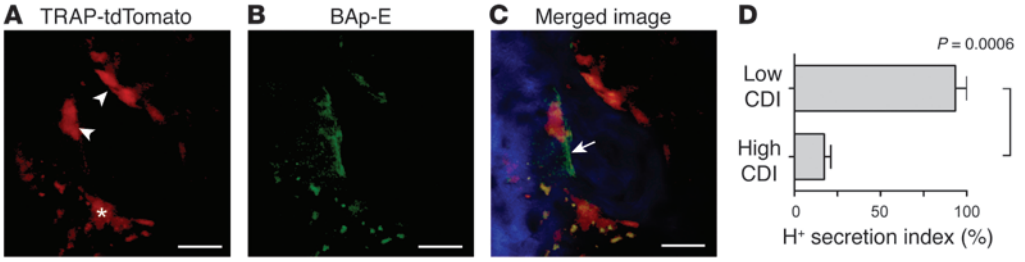

Figure 3
Visualization of bone-resorptive function of mature osteoclasts by using H+-sensing fluorescent probe. (**A**–**C**) Representative images from intravital multiphoton imaging of mouse bone tissues of heterozygous TRAP-tdTomato transgenic mice treated with BAp-E, an H+ probe detecting sites of local bone resorption (Supplemental Video 5). Mature osteoclasts expressing TRAP-tdTomato signals (**A**), green fluorescent signals from high H+ concentration (**B**), and merged images (**C**). Green fluorescent signals from the H+ probes overlapped with static (low CDI, arrowheads) but not moving (high CDI, asterisk) osteoclasts, suggesting that former cells are secreting protons actively and resorbing bone tissues when observed in vivo. Some green fluorescent signal (**C**, arrow) could also be detected along the bone surfaces near to static osteoclasts. Given the rate of transition from static to motile behavior of the osteoclasts, these areas are likely to be those undergoing resorption by previously static cells shortly before obtaining the image and characterizing the osteoclasts at motile. Scale bars: 40 μm. (**D**) The H+ secretion index of mature osteoclasts. The H+ secretion index was defined as the ratio of the number of osteoclasts overlapping with green fluorescent acid pH signals divided by the total number of osteoclasts of the indicated type that were imaged (n = 3, from 3 independent experiments).

(0.1 mg/kg), which is not sufficient for promoting osteoclastogenesis in vivo (not shown), could also efficiently convert N into R states in vivo (Figure 4D), suggesting that the level of RANKL required for N-to-R conversion may be lower than that necessary for inducing differentiation or maturation during osteoclastogenesis, with intriguing implications for control of bone state. In these experiments, unlike the cases with long exposure with RANKL (in Figure 2A), we could not observe the differences in subcellular distribution of V$^-$-type H$^+$-ATPases shown in Figure 1, B and C, suggesting that it may take a substantial (more than 10 to 20 minutes) period for relocalization of these proteins to support highly active bone resorption. We determined that i.v. injection of GST did not significantly change the average cell motility for up to 40 minutes (Figure 4D).

Osteoclastogenic RANKL is mainly supplied from osteoblasts, osteocytes, and/or stromal cells in bone marrow, although RANKL has also been reported to be expressed by diverse immune cell types such as T lymphocytes (24, 25). Among several T cell subtypes, CD4$^+$ Th17 cells, which are associated with autoimmune disorders including rheumatoid arthritis, have been reported to express RANKL on the cell surface (26). However, the in vivo function of RANKL on Th17 is not clear because the expressed RANKL exhibited little ability to induce osteoclastogenesis in vitro. We therefore looked for a possible physical and functional relationship between RANKL-bearing Th17 cells and mature osteoclasts in vivo by visualizing these cells simultaneously in intact bones (Figure 5A). Polyclonal Th17 and Th1 cells

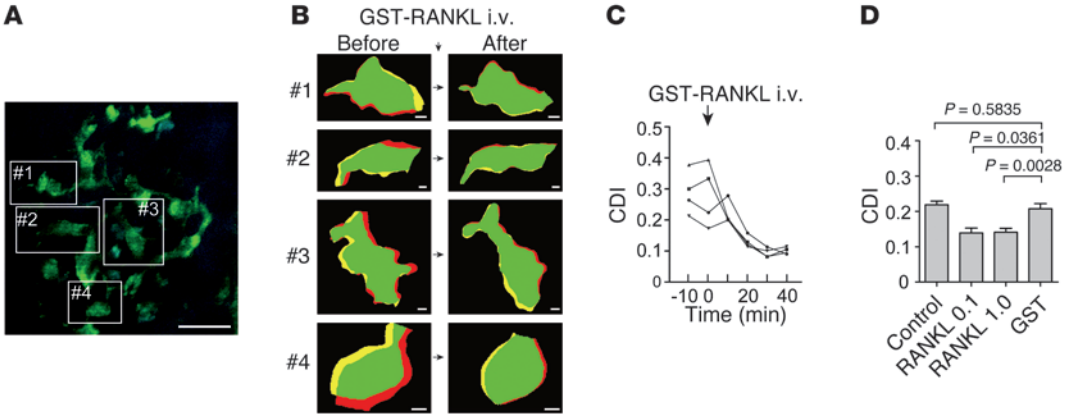

Figure 4
RANKL-mediated rapid control of mature osteoclast function. (**A**) Intravital multiphoton imaging of osteoclasts in mouse bone tissues of a3-GFP mice under control conditions (Supplemental Video 6). Mature osteoclasts expressing GFP-fused V-type H+ ATPase a3 subunit are in green. Blue, bone surface. Cell borders are marked in white lines. Scale bar: 40 μm. (**B**) Representative computer-processed images of mature osteoclasts and their RANKL-mediated rapid shape changes. Images 1–4 were computer extracted from images under the initial condition from **A** (left panels) and again 10 minutes after i.v. injection of 1 mg/kg of GST-RANKL (right panels) (as in Figure 1, E and F). Scale bars: 5 μm. (**C**) Representative time courses of the CDI for the 4 individual cells shown in **B**. Moving (high CDI) osteoclasts underwent transition to the static (low CDI) state less than 10 minutes after i.v. administration of RANKL. (**D**) The summary of CDIs under control conditions (control) and 40 minutes after i.v. injection of 0.1 mg/kg of GST-RANKL (RANKL 0.1), 1 mg/kg of GST-RANKL (RANKL 1), or GST alone (n = 13 for control, n = 5 for 0.1 mg/kg of GST-RANKL, n = 13 for 1 mg/kg of GST-RANKL, and n = 21 for GST alone, compiled from 3 independent experiments).

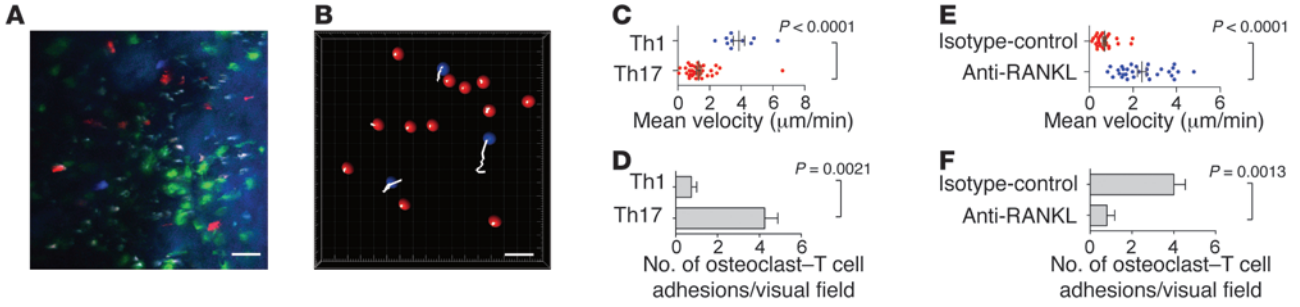

Figure 5

The interaction between Th17 and osteoclast depends on RANKL expressed on Th17. (**A**) Intravital multiphoton imaging (low-power view) of osteoclasts (green) in mouse bone tissues of a3-GFP mice after administration of in vitro–differentiated Th1 (labeled with CMF_2HC — blue) and Th17 (labeled with CMTPX — red) (Supplemental Video 7). Cell borders are marked by white lines. Scale bar: 40 μm. (**B**) The migratory behaviors of Th1 and Th17. Blue and red spheres represent Th1 and Th17 cells, respectively, and white lines show the associated trajectories. Scale bar: 40 μm. (**C**) Summary of mean tracking velocities of Th1 and Th17 cells. Data points (n = 10 for Th1, and n = 48 for Th17) represent individual cells compiled from 3 independent experiments. (**D**) The number of Th1 or Th17 cells attached to mature osteoclasts for more than 5 minutes (n = 4, from 3 independent experiments). (**E**) Summary of mean tracking velocity of Th17 cells treated with isotype control antibody or anti-RANKL antibody. Data points (n = 32 for Th17 cells treated with isotype control antibody and n = 30 for Th17 cells treated with anti-RANKL antibody) represent individual cells compiled from 3 independent experiments. (**F**) The number of Th17 cells treated with isotype control antibody or anti-RANKL antibody attached to mature osteoclasts for more than 5 minutes (n = 5, from 3 independent experiments).

were differentiated in vitro using appropriate sets of cytokines and neutralizing antibodies (ref. 26 and Supplemental Figure 4), stained with cell-permeable fluorescent dyes, CMTPX (red) and CMF_2HC (blue), respectively, and then adoptively transferred i.v. into a3-GFP mice shortly before imaging (Figure 5, A and B, and Supplemental Video 7). Th17, but not Th1, preferentially adhered to mature osteoclasts (Figure 5, C and D) under these conditions, even though both Th cells migrated into bone marrow cavity to the same extent (Supplemental Figure 5A). Pretreatment of Th17 with anti-RANKL neutralizing antibody (27, 28) or osteoprotegerin (OPG), a decoy receptor for RANKL (29), reduced association of these T cells with the osteoclasts (Figure 5, E and F, Supplemental Figure 6, and Supplemental Video 8), whereas we observed no effect of anti-RANKL on the mobility of Th1 cells (Supplemental Figure 7). These results suggest that the interaction between Th17 and osteoclast is at least partly dependent on RANKL expressed on the surface of Th17, although we cannot exclude the possibility that additional molecules may play a role in this colocalization. Moreover, we found that mature osteoclasts adherent to Th17 were R, as compared with nonconjugated cells (Figure 6, A and C), and that N osteoclasts were converted to static ones shortly after conjugation with Th17 (Figure 6, D–F, and Supplemental Video 9).

We further examined the role of Th17 in osteoclastic bone resorption using the pH probe (BAp-E) to detect local pH changes in vivo (Figure 3). Either Th17 or Th1 cells were labeled with CMTPX (red) and then transferred to the mice pretreated with BAp-E. Th17 cells seemed to be closely adjacent to green signals from BAp-E representing acidic areas (Figure 6G), whereas Th1 cells were not present in proximity to these indicator signals (Figure 6G). Figure 6H shows the ratio of the number of Th1 or Th17 cells close to the low pH signals divided by the total number of Th1 or Th17 cells in visual fields. These data indicate a preferential association between the location of Th17 T cells and sites of pH drop and support our concept that Th17, but not Th1, mediates bone-resorptive acid secretion from mature osteoclasts at local sites of T cell–osteoclast contact. Taken together, these results reveal a new function of RANKL-expressing Th17, namely stimulation of bone resorption by converting nonresorbing to resorbing mature osteoclasts on the bone surface in situ.

Discussion

Bone tissue sectioning accompanied with conventional histomorphometric analyses has been the major methodology employed to date for studying bone resorption and osteoclast function in vivo (30) and has provided substantial insight into functional aspects of bone physiology. Here we applied 2-photon microscopy to attain previously unavailable insight into the in vivo dynamic behavior of osteoclasts on the bone surface, detailing for what we believe is the first time how osteoclast movement and resorptive function are related as well as how this activity is modulated by cytokines, immune cells, and pharmacologic agents. Our imaging studies have revealed that osteoclasts on the bone surface show substantial heterogeneity in motility and rapid transitions in this motility in conjunction with alternation in their functional states. RANKL administration or direct interaction with RANKL-bearing Th17 cell appears to stimulate local bone resorption by dynamically modulating the linked changes in migratory status and function of osteoclasts within a short period (10~20 minutes).

While it provides information on osteoclast behavior and activity in situ, data from this method must be compared with caution to results derived from other techniques. Previous studies using conventional bone histomorphometry showed that bisphosphonate treatment stimulates osteoclast formation in mice (31), findings that are in seeming conflict with the present results shown in Figure 2C. Our own studies using bone sectioning with TRAP staining to examine the effect of risedronate in a3-GFP mice have also shown that the total number of mature osteoclasts slightly increased, compared with control conditions (not shown). Moreover, we could find some larger $a3\text{-}GFP^+TRAP^+$ double-positive osteoclasts in treated mice, in accord with previous results demonstrating an increase in giant osteoclasts in bisphosphonate-treated bone specimens (31). Multiphoton imaging, as we use it here, provides 2D scanning on the bone

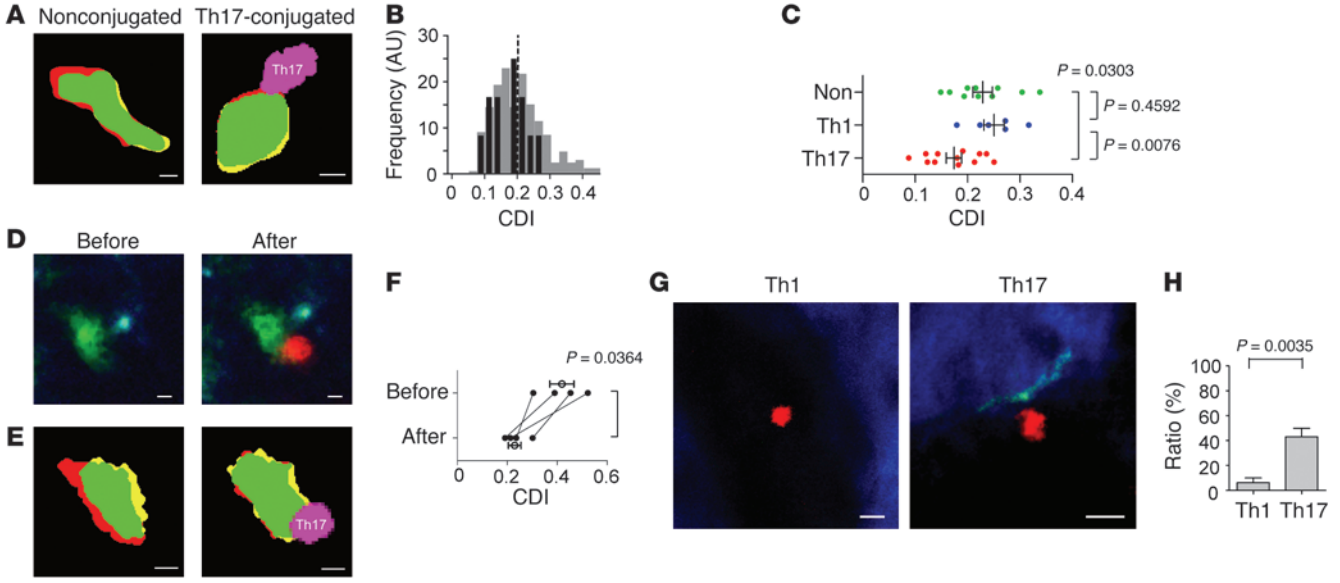

Figure 6

Regulation of mature osteoclast function by RANKL expressed on Th17. (**A**) Mature osteoclasts (green/red/yellow) either alone or in conjugate with Th17 (magenta); corresponding CDIs were determined (see details in Figure 1D). Scale bars: 5 μm. (**B**) Histogram of CDIs of mature osteoclasts conjugated with Th17 (black) and under control conditions (gray, same as in Figure 1H). (**C**) Summary of the CDIs of mature osteoclasts alone or conjugated with Th1 or Th17 (n = 10 for nonconjugated [Non], n = 6 for Th1-conjugated [Th1], and n = 12 for Th17-conjugated [Th17]). (**D**) A representative image showing a migrating Th17 contacting a mature osteoclast. Green, mature osteoclast; red, Th17. Scale bar: 5 μm. (**E**) Change in osteoclast motility associated with Th17 contact. The CDIs before (left) and after (right) conjugation with Th17 are depicted. Magenta, Th17. Scale bars: 5 μm. (**F**) Summary of CDI changes corresponding to Th17 conjugation (n = 4). Moving (high CDI) osteoclasts underwent transition into static (low CDI) states 20 minutes after conjugation with Th17. (**G**) Representative images of live bone imaging of wild-type mice treated with BAp-E. In vitro–differentiated Th1 (left) or Th17 (right) were labeled with CMTPX (red) and then transferred as independent. Fluorescent signals from high H^+ concentration are in green. Blue, bone surface. Scale bar: 10 μm. (**H**) The ratio of the number of Th1 or Th17 attached to the BAp-E divided by the total number of Th1 or Th17 (n = 4). Each experiment was performed independently at least 3 times.

surface in a focal plane, whereas the bone surface is represented by 1D "lines" along the bone trabeculae in classical histomorphometrical analyses. Cell shapes and the appearance of mature osteoclasts in these 2 analysis systems are quite different. Perhaps of greatest importance is that the present imaging method specifically detects only those osteoclasts tightly adherent to the bone surface and not cells that may be near this surface but not firmly bound. The majority of mature osteoclasts in bisphosphonate-treated mice may be slightly detached from the surface (32) and thus not quantified in our imaging. These considerations suggest a cautious approach to interpretation of all imaging data; in the present case, the method is best suited to the dynamic and functional analysis of strongly bone adherent osteoclasts and not all such cells in the marrow, and our interpretations are based on this adherent subpopulation.

RANKL is generally considered to be a critical factor in the terminal differentiation of osteoclasts. Here, we show RANKL also plays roles in regulating the bone-resorptive function of fully differentiated "mature" osteoclasts (Supplemental Figure 8). This finding is consistent with maintenance of expression of RANK, a receptor for RANKL, on mature osteoclasts. This contrasts with expression of CSF1R or CX_3CR1, which is necessary for differentiation or positioning of osteoclasts and their precursors, but becomes dispensable in the late phase of osteoclastogenesis and which is downregulated after maturation. Importantly, this newly identified effect of RANKL is seen with a lower amount of RANKL than that required for stimulating de novo osteoclastogenesis, and it appears that the amount expressed on Th17 is indeed sufficient for this effect. There have been a series of reports indicating a critical contribution of Th17 in bone-resorptive inflammatory diseases, such as rheumatoid arthritis, although the molecular mechanism by which these T cells contribute to pathogenesis has been unresolved (33, 34). Th17 accumulation in synovial fluid (35) may contribute to arthritic bone erosion partly by stimulating mature osteoclasts in such a manner. Overall, our findings clearly demonstrate an unanticipated cycling of mature osteoclasts between active, bone-resorptive and static, inactive states as well as key molecular and cellular players involved in changing the relative proportion of the 2 osteoclast types at the bone surface. This resorption switching on the bone surface in situ may represent an interesting therapeutic target.

Methods

Mice. The generation of the V-type H^+ ATPase a3 subunit-GFP fusion knockin mice was described previously (13). For the generation of the TRAP promoter-tdTomato transgenic mice, tdTomato cDNA (Clontech) was inserted into an pL451 vector containing an Frt-PGK-promoter-Neo-Frt cassette. Recombination protocol was carried out as described (36). Briefly, forward primer (5′-TAGTGCCTGAGTTTATAGGCATGCACCGTGAGACCAGGCTCAGCGGGCTAGTCTTTCTTTGCTTGGACCAGGGTCTCGCTCTCTGTCCTCACCAGAGACTCTGAACTCCCTCTCTTCCTCACAG**ATG**GTGAGCAAGGGCGAGGAGGTCA-3′) and reverse primer (5′-CATTGGGGACCCCTCCCCAGTCGCCCACAGCCACAAATCTCAGGGTGGGAGTGGGGGCTGTACCGTGGGTCAG-

GAGTGGGAGCCATATGATTTGTAGGCCCAGCAGCACCACCCATGAATCAGTTATATTATGTACCTGACTGAT-3′) were used to amplify a fragment containing tdTomato cDNA as well as the homologous sequences flanking the mouse TRAP ATG start codon site. The underlined sequences of these primers were matching to the sequences before and after the start codon ATG (bold) of TRAP. The resulting PCR product was transfected into the SW105 bacteria carrying RP24-75C9 according to the standard procedure as described previously. The kanamycin-resistant clones were further screened using PCR screening protocols. The Frt-PGK-promoter-Neo-Frt cassette in positive BAC clones was deleted by inducing FLP recombinase followed by confirmation using BAC DNA sequencing (Supplemental Figure 9). The purified RP24-75C9-TRAP-tdTomato was microinjected into the pronucleus of C57BL/6 fertilized eggs. Southern blot was employed to identify the potential founder mice using a tdTomato DNA fragment as a probe. A DNA dot bolt was carried out to determine the specificity of this tdTomato probe using the plasmids containing tdTomato or other cDNA. All mice were bred and maintained under specific pathogen–free conditions at animal facilities of Osaka University and NIH. We confirmed that both a3-GFP knockin and TRAP-tdTomato transgenic mice had no abnormality in terms of bone homeostasis by using bone morphometrical analyses.

Multiphoton intravital bone tissue imaging. Intravital microscopy of mouse calvaria bone tissues was performed using a protocol modified from a previous study (7, 8). Ten- to fourteen-week-old mice were anesthetized with isoflurane (Escain; 2.0% vaporized in 100% oxygen), the frontoparietal regions of the skull bones were exposed, and then the internal surfaces of bones adjacent to bone marrow cavity were observed by using multiphoton excitation microscopy. The imaging system was composed of a multiphoton microscope (SP5; Leica) driven by a laser (Mai-Tai HP Ti: Sapphire; Spectraphysics) tuned to 840–900 nm and an upright microscope (DM6000B; Leica) equipped with a ×20 water immersion objective (HCX APO, N.A. 1.0; Leica). Fluorescent cells were detected through band-pass emission filters at 525/50 nm (for GFP and BAp-E), at 455/50 nm (for CMF_2HC), and at 585/40 nm (for CMTPX). Vessels were visualized by injecting 70 kDa of Texas red–conjugated dextran (detected using a 585/40 nm filter) i.v. immediately before imaging. Image stacks were collected at 5-μm vertical step size at a depth of 100–150 μm below the skull bone surface. Raw imaging data was processed with Imaris (Bitplane) with a Gaussian filter for noise reduction. Image drifts were corrected by using image analysis software, Imaris or CL-Quant 2.30 (Nikon), according to a standard protocol.

Chemical synthesis of H^+ sensing fluorescent probe. The chemical synthesis of BAp-E, a fluorescent probe detecting H^+ secretion was described previously (21).

Image data analysis. Assessment of the R state and N state of mature osteoclasts was performed by using newly developed image analysis software CL-Quant 2.30 (Nikon) (37) for tracking the morphological changes of mature osteoclasts. The details of how we defined the R and N states are described in Supplemental Figure 2 and Supplemental Video 2.

Treatment with RANKL and bisphosphonate. In some experiments, a3-GFP mice were treated with GST-RANKL and/or risedronate. GST-RANKL (Oriental Yeast) (1 mg/kg) dissolved in PBS was injected intraperitoneally into a3-GFP female mice 2 days before imaging. 10 μg/kg of risedronate (17) (provided by Ajinomoto Pharmaceuticals Co.) dissolved in PBS was subcutaneously injected into the mice every day beginning 5 days prior to taking images. GST (1 mg/kg) dissolved in PBS was also injected as a control. For examining short-term effects of RANKL, GST-RANKL (1 or 0.1 mg/kg) or GST (1 mg/kg) dissolved in PBS were administered i.v. during imaging, and images were acquired consecutively.

In vitro differentiation of $CD4^+$ T cells. $CD4^+$ T cells were purified from the spleen and peripheral lymph nodes of wild-type mice by using Dynabeads FlowComp Mouse $CD4^+$ Isolation Kit (Life Technologies). The purity of the $CD4^+$ T cells was greater than 95%. These $CD4^+$ T cells were cultured with a plate-bound 1 μg/ml anti-CD3 mAb (Biolegend) and 1 μg/ml anti-CD28 mAb (Biolegend) and differentiated into Th1 or Th17 cells, in the presence of 10 μg/ml anti–IL-4 mAb (R&D) and 10 ng/ml IL-12 (PeproTech), or 10 μg/ml anti–IFN-γ mAb (R&D), 10 μg/ml anti–IL-4 mAb, and 10 ng/ml IL-23 (R&D), respectively. After incubation for 3 days, cells were collected and checked for differentiation into Th1 or Th17, by using flow cytometry and RT-PCR. In vitro differentiated Th1 or Th17 cells were labeled with CMF_2HC (50 μM; Life Technologies) and CMTPX (15 μM; Life Technologies), respectively. In some experiments, Th1 or Th17 cells were incubated with 1 μg/ml anti-mouse RANKL neutralizing mAb (Oriental Yeast), OPG (R&D), or rat IgG2a, κ isotype control antibody (BD Biosciences — Pharmingen) at 4°C for 15 minutes and labeled with CMTPX (15 μM) or CMF_2HC (50 μM). After labeling, each cell was transferred to a3-GFP mice. Two hours, later mouse skull bone tissues were observed by using intravital multiphoton microscopy, as previously described.

Immunohistochemistry. Immunohistological analyses were performed as described previously (7). Fluorescence-based staining for TRAP with ELF97 substrate (Life Technologies) was used with some modifications.

Quantitative real-time PCR. Quantitative real-time PCR was performed with Thermal Cycler Dice Real Time System TP800 (Takara) using the following specific primer pairs: Rorγt (5′-GCCGCGGAGCAGACACACTT-3′ and 5′-GCTGCAGCCCAAGGCTCGAA-3′), RANKL (5′-GTACCTGCGCAGCTCGGAGG-3′ and 5′-GCCTCAGGCTTGCCTCGCTG-3′), and GAPDH (5′-ACCACAGTCCATGCCATCAC-3′ and 5′-TCCACCACCCTGTTGCTGTA-3′).

Flow cytometry. All reagents were purchased from BD. To examine the existence of transferred Th1 and Th17 cells in spleen and bone marrow of a3-GFP mice, splenocytes and bone marrow cells were collected from the mice after taking images. To confirm the cell-surface expression of RANKL on T cells, in vitro differentiated Th1 and Th17 cells were first incubated with anti-mouse CD16/32 antibody (eBioscience) to block nonspecific binding, followed by incubation with either PE-conjugated rat anti-mouse RANKL antibody (BD Pharmingen) or PE-conjugated rat IgG2a, κ isotype control (BioLegend). Flow cytometric data were collected on a FACSCanto II (BD) and analyzed with FlowJo software (Tree Star).

Statistics. The Mann–Whitney rank sum test was used to calculate *P* values for highly skewed distributions. For Gaussian-like distributions, 2-tailed *t* tests were used. Data represent mean ± SEM unless otherwise specified. $P < 0.05$ was considered significant.

Study approval. All animal experiments were performed according to institutional animal experimental guidelines under approved protocols from the Animal Experimental Committee of Osaka University and the National Institute of Allergy and Infectious Diseases (NIAID) Institutional Animal Care and Use Committee.

Acknowledgments

We thank Y. Shimazu and A. Kubo for experimental assistance. This work was supported by Grants-in-Aid for Encouragement of Young Scientists (A) (no. 22689030), for Scientific Research on Innovative Areas (no. 22113007); by a Funding Program for World-Leading Innovative R&D on Science and Technology (FIRST Program) from the Ministry of Education, Science, Sports and Culture of Japan; by a Grant-in-Aid for Research on Allergic Disease and Immunology (H21-010) from the Ministry of Health, Labor and Welfare of Japan; by a grant from the International Human Frontier Science Program (CDA-00059/2009 and RGY0077/2011); and by grants from the Takeda Science Founda-

tion, the Mochida Memorial Foundation for Medical and Pharmaceutical Research, the Astellas Foundation for Research on Metabolic Disorders, the Kanae Foundation for the Promotion of Medical Science, the Pfizer Health Research Foundation, and the Uehara Memorial Foundation. It was also supported by the Intramural Research Program, NIAID, NIH.

Received for publication September 28, 2012, and accepted in revised form November 29, 2012.

Address correspondence to: Masaru Ishii, Laboratory of Cellular Dynamics, Immunology Frontier Research Center, Osaka University, 3-1 Yamada-oka, Suita, Osaka 565-0871, Japan. Phone: 81.6.6879.4268; Fax: 81.6.6879.8296; E-mail: mishii@ifrec.osaka-u.ac.jp.

Ge-Hong Sun-Wada's present address is: Department of Biochemistry, Faculty of Pharmaceutical Sciences, Doshisha Women's College, Kyoto, Japan.

1. Teitelbaum SL, Ross FP. Genetic regulation of osteoclast development and function. *Nat Rev Genet*. 2003;4(8):638–649.
2. Karsenty G, Wagner EF. Reaching a genetic and molecular understanding of skeletal development. *Dev Cell*. 2002;2(4):389–406.
3. Takahashi N, et al. Osteoclast-like cell formation and its regulation by osteotropic hormones in mouse bone marrow cultures. *Endocrinology*. 1988; 122(4):1373–1382.
4. Roodman GD, Windle JJ. Paget disease of bone. *J Clin Invest*. 2005;115(2):200–208.
5. Turcotte RE. Giant cell tumor of bone. *Orthop Clin North Am*. 2006;37(1):35–51.
6. Mazo IB, et al. Bone marrow is a major reservoir and site of recruitment for central memory CD8+ T cells. *Immunity*. 2005;22(2):259–270.
7. Ishii M, et al. Sphingosine-1-phosphate mobilizes osteoclast precursors and regulates bone homeostasis. *Nature*. 2009;458(7237):524–528.
8. Ishii M, Kikuta J, Shimazu Y, Meier-Schellersheim M, Germain RN. Chemorepulsion by blood S1P regulates osteoclast precursor mobilization and bone remodeling in vivo. *J Exp Med*. 2010; 207(13):2793–2798.
9. Blair HC, Teitelbaum SL, Ghiselli R, Gluck S. Osteoclastic bone resorption by a polarized vacuolar proton pump. *Science*. 1989;245(4920):855–857.
10. Nakamura H, Moriyama Y, Futai M, Ozawa H. Immunohistochemical localization of vacuolar H(+)-ATPase in osteoclasts of rat tibiae. *Arch Histol Cytol*. 1994;57(5):535–539.
11. Toyomura T, Oka T, Yamaguchi C, Wada Y, Futai M. Three subunit a isoforms of mouse vacuolar H(+)-ATPase. Preferential expression of the a3 isoform during osteoclast differentiation. *J Biol Chem*. 2000; 275(12):8760–8765.
12. Toyomura T, et al. From lysosomes to the plasma membrane: localization of vacuolar-type H+ -ATPase with the a3 isoform during osteoclast differentiation. *J Biol Chem*. 2003;278(24):22023–22030.
13. Sun-Wada GH, Tabata H, Kawamura N, Aoyama M, Wada Y. Direct recruitment of H+-ATPase from lysosomes for phagosomal acidification. *J Cell Sci*. 2009;122(pt 14):2504–2513.
14. Nishi T, Forgac M. The vacuolar (H+)-ATPases — nature's most versatile proton pumps. *Nat Rev Mol Cell Biol*. 2002;3(2):94–103.
15. Frattini A, et al. Defects in TCIRG1 subunit of the vacuolar proton pump are responsible for a subset of human autosomal recessive osteopetrosis. *Nat Genet*. 2000;25(3):343–346.
16. Karsdal MA, Martin TJ, Bollerslev J, Christiansen C, Henriksen K. Are nonresorbing osteoclasts sources of bone anabolic activity? *J Bone Miner Res*. 2007;22(4):487–494.
17. Tomimori Y, et al. Evaluation of pharmaceuticals with a novel 50-hour animal model of bone loss. *J Bone Miner Res*. 2009;24(7):1194–1205.
18. Soysa NS, et al. The pivotal role of the alternative NF-kappaB pathway in maintenance of basal bone homeostasis and osteoclastogenesis. *J Bone Miner Res*. 2010;25(4):809–818.
19. Reszka AA, Rodan GA. Mechanism of action of bisphosphonates. *Curr Osteoporos Rep*. 2003; 1(2):45–52.
20. Russell RG, et al. Bisphosphonates: an update on mechanisms of action and how these relate to clinical efficacy. *Ann N Y Acad Sci*. 2007;1117:209–257.
21. Kowada T, et al. In vivo fluorescence imaging of bone-resorbing osteoclasts. *J Am Chem Soc*. 2011; 133(44):17772–17776.
22. Nakayama T, et al. Polarized osteoclasts put marks of tartrate-resistant acid phosphatase on dentin slices — a simple method for identifying polarized osteoclasts. *Bone*. 2011;49(6):1331–1339.
23. Burgess TL, et al. The ligand for osteoprotegerin (OPGL) directly activates mature osteoclasts. *J Cell Biol*. 1999;145(3):527–538.
24. Kong YY, et al. Activated T cells regulate bone loss and joint destruction in adjuvant arthritis through osteoprotegerin ligand. *Nature*. 1999; 402(6759):304–309.
25. Takayanagi H, et al. T-cell-mediated regulation of osteoclastogenesis by signalling cross-talk between RANKL and IFN-gamma. *Nature*. 2000; 408(6812):600–605.
26. Sato K, et al. Th17 functions as an osteoclastogenic helper T cell subset that links T cell activation and bone destruction. *J Exp Med*. 2006; 203(12):2673–2682.
27. Asselin-Labat ML, et al. Control of mammary stem cell function by steroid hormone signalling. *Nature*. 2010;465(7299):798–802.
28. Furuya Y, et al. Increased bone mass in mice after single injection of anti-receptor activator of nuclear factor-kappaB ligand-neutralizing antibody: evidence for bone anabolic effect of parathyroid hormone in mice with few osteoclasts. *J Biol Chem*. 2011; 286(42):37023–37031.
29. Simonet WS, et al. Osteoprotegerin: a novel secreted protein involved in the regulation of bone density. *Cell*. 1997;89(2):309–319.
30. Parfitt AM, et al. Bone histomorphometry: standardization of nomenclature, symbols, and units. Report of the ASBMR Histomorphometry Nomenclature Committee. *J Bone Miner Res*. 1987;2(6):595–610.
31. Matsumoto T, et al. Distinguishing the proapoptotic and antiresorptive functions of risedronate in murine osteoclasts: role of the Akt pathway and the ERK/Bim axis. *Arthritis Rheum*. 2011; 63(12):3908–3917.
32. Kuroshima S, Go VA, Yamashita J. Increased numbers of nonattached osteoclasts after long-term zoledronic acid therapy in mice. *Endocrinology*. 2012;153(1):17–28.
33. Adamopoulos IE, Bowman EP. Immune regulation of bone loss by Th17 cells. *Arthritis Res Ther*. 2008; 10(5):225.
34. Peck A, Mellins ED. Breaking old paradigms: Th17 cells in autoimmune arthritis. *Clin Immunol*. 2009;132(3):295–304.
35. Takayanagi H. Osteoimmunology and the effects of the immune system on bone. *Nat Rev Rheumatol*. 2009;5(12):667–676.
36. Lee EC, et al. A highly efficient Escherichia coli-based chromosome engineering system adapted for recombinogenic targeting and subcloning of BAC DNA. *Genomics*. 2001;73(1):56–65.
37. Alworth SV, Watanabe H, Lee JS. Teachable, high-content analytics for live-cell, phase contrast movies. *J Biomol Screen*. 2010;15(8):968–977.